*Key Engineering Materials*
*ISSN: 1662-9795, Vol. 926, pp 2183-2192*
*doi:10.4028/p-3a8e45*

*Submitted: 2021-12-08*
*Revised: 2022-01-28*
*Accepted: 2022-01-30*
*Online: 2022-07-22*

# Calibration of the Elasto-Plastic Properties of Friction Stir Welded Blanks in Aluminum Alloy AA6082

Fausto TUCCI[1,a*], Antonio ANDRADE CAMPOS[2,b], Sandrine THUILLIER[3,c] and Pierpaolo CARLONE[1,d]

[1]Department of Industrial Engineering, University of Salerno, 132, via Giovanni Paolo II, 84084, Fisciano (SA), Italy

[2]Center for Mechanical Technology and Automation, Dep. Mechanical Engineering, University of Aveiro, 3810-190 Aveiro, Portugal

[3]Univ. Bretagne Sud, UMR CNRS 6027, IRDL, F-56100 Lorient, France

[a]ftucci@unisa.it, [b]gilac@ua.pt, [c]sandrine.thuillier@univ-ubs.fr, [d]pcarlone@unisa.it

**Keywords:** friction stir welding; aluminum alloy; AA6082-T6; constitutive law calibration; microhardness.

**Abstract.** In recent years remarkable efforts have been devoted to the study of the formability of tailored blanks processed by friction stir welding (FSW) by means of numerical and experimental approaches.
This study aims to perform an inverse analysis to calibrate the constitutive law of FSW blanks produced with different parameters. The evaluated mechanical behavior will be employed in future studies to investigate the formability of such elements by single point incremental forming. Friction stir welded blanks in aluminum alloy AA6082-T6 produced with different advancing velocities and tool rotational speeds have been considered. Specimens for tensile testing have been cut and collected from the FSW blanks. The longitudinal dimension of the specimens was perpendicular to the tool advancing direction, with the welding centerline located at the middle point of the coupon. From the same welded blanks further specimens have been collected to conduct microhardness testing of the cross-section in the welding zone.
Data from digital image correlation (DIC) have been adopted to detect the zones of local variation of the mechanical properties related to the peculiar microstructure determined by friction stir welding. In particular, the data were used as input to feed an iterative numerical procedure to calibrate the constitutive law variable as a function of the distance from the welding centerline.

## Introduction

Industry and designers are constantly requesting lighter, more resistant, better adaptable materials to reduce fuel consumption in automotive and aerospace sectors, to better combine dissimilar materials, to enhance the surface properties or to produce lighter structures [1–10]. This necessity is met in many cases by using advanced composite materials [11–20]. Nevertheless, in some cases, the need for customized local properties cannot be effectively met by fiber reinforced polymers. To fulfill these necessities, tailored blanks have been conceptualized and developed. These components are sheets in metal alloy with mechanical, physical and chemical local behaviors achieved combining different materials, applying local surface treatments, and/or providing local forming processes [21].

The combination of different materials is not achievable by conventional joining techniques. The friction stir welding (FSW) is a solid state joining process adopted to produce similar or dissimilar connection in different joint configurations [22–24]. In FSW, the rotation of a cylindrical tool penetrating the parts to be connected mixing the crystal lattices of the base materials, determining a mechanical interlock at solid state, below the melting points of the processed alloys. The cylindrical tools in HSS are mounted within the rotating mandrels of computerized-numerical-control machines, which controls its rotation, plunging, and advancements. The thermo-mechanical action of the rotating and advancing tool determining the joining of the parts give place to a particular stratified microstructure in which at least four different regions can be detected: the nugget zone, the thermo-

mechanically affected zone, the heat affected zone, and the base material. The elastoplastic properties as well as the microhardness variates in the different zones according to the local microstructural morphology [22,23].

Typically, the tailored blanks present complex shapes, therefore, the flat sheets must be formed using plastic deformation processes. One of the most employed deformation processes for tailored blanks is the single point incremental forming due to its high formability performances and its versatility [25]. Recently, several studies focused on the plastic properties of FSW blanks in aluminum alloys [26,27]. The experimental evidence demonstrates that their elastoplastic behavior is sensibly influenced by the tool rotational speed and the advancing velocity adopted during FSW. Single point incremental forming processes of friction stir welded tailored blanks in aluminum alloy in butt joint configuration demonstrated that with a proper choice of the process parameters the welding line presents a better formability than the base material [28,29].

Aiming to experimentally evaluate the variability of the elastoplastic behavior, tensile tests are typically performed on samples collected perpendicularly to the welding line. The study of the local deformation by digital image correlation technique provided the data to define a constitutive law with the parameters as a function of the distance from the weld line [29].

Several works in literature focused on the correlation between mechanical properties and material hardness. The topic is still not completely explored and an unique theory does not exist currently [30]. Nevertheless, research has been produced analyzing material indentation mechanisms with analytical and numerical analyses [31]. Typically, this kind of analyses are devoted to developing synthetic black-box models to determine the hardness of a sample providing as input the elastic modulus, the yield stress, and the hardening factor of the materials.

The work described in the present article aims to calibrate the constitutive law of friction stir welded blanks in aluminum alloy AA6082 T6. The joints produced by FSW using different tool rotational speeds and advancing velocities have been assessed by tensile testing transversally to the welding line. Digital image correlation technique has been adopted to detect and measure the local stress-strain behavior. Microhardness tests have been performed on the cross-section of the produced blanks.

## Materials and Methods

Blanks in aluminum alloy AA6082 T6 having thickness of 2 mm have been used for the present experimental work. Strips of 110 mm in width and 220 in length have been collected from a rolled sheet. Such strips have been joined by FSW along the 220 mm long edge, giving place to square welded blanks having edges of 220 mm. The FSW has been performed using a Famup MCX 600 CNC machine equipped with a HSS cylindrical tool presenting a conical pin (Fig. 1(a)). The geometrical features of the tool are described in Table 1.

*Table 1. Geometrical features of the HSS friction stir welding tool.*

| Geometrical parameter | Value |
|---|---|
| Shoulder diameter | 20 [mm] |
| Conic pin angle | 15° |
| Pin height | 1.8 [mm] |
| Pin minimum diameter | 3.8 [mm] |

Aiming to investigate and analyze the effects of the FSW thermo-mechanical loads in relation with the adopted parameters, the welding processes have been performed in five different conditions of advancing velocity and tool rotational speed. The adopted conditions are schematically detailed in Fig. 1(b).

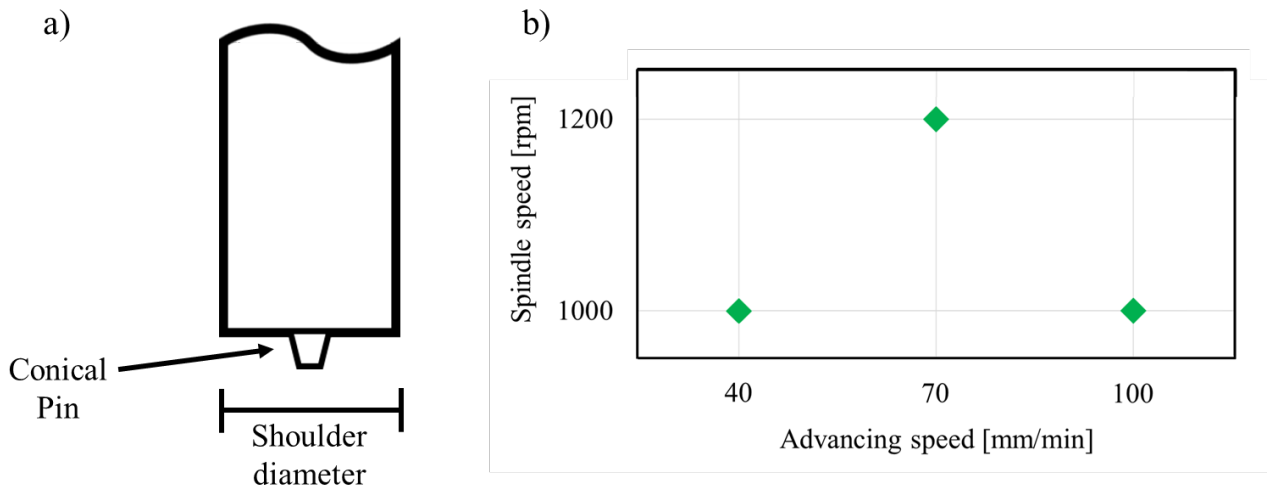


*Figure 1. a) Representation of the friction stir welding tool; b) adopted process parameters.*

The strips were fixed to the CNC machine working plan by rigid clamps, placing adjacent the long edge of two strips to form a butt joint configuration. A tool plunging of 2 mm was set. For each of the welding parameters, two repetitions were performed.

The welded blanks were cut to extract samples for tensile testing and microhardness indentation. Samples for tensile testing were collected transversally to the welding line, having the welding centerline at their middle length. Digital image correlation (DIC) has been used during tensile testing to acquire the local elasto-plastic behaviors of the samples. The properties identification has been carried out by using the finite element model updating (FEMU) approach. This procedure is based on the iterative procedure, schematically described in Figure 2.

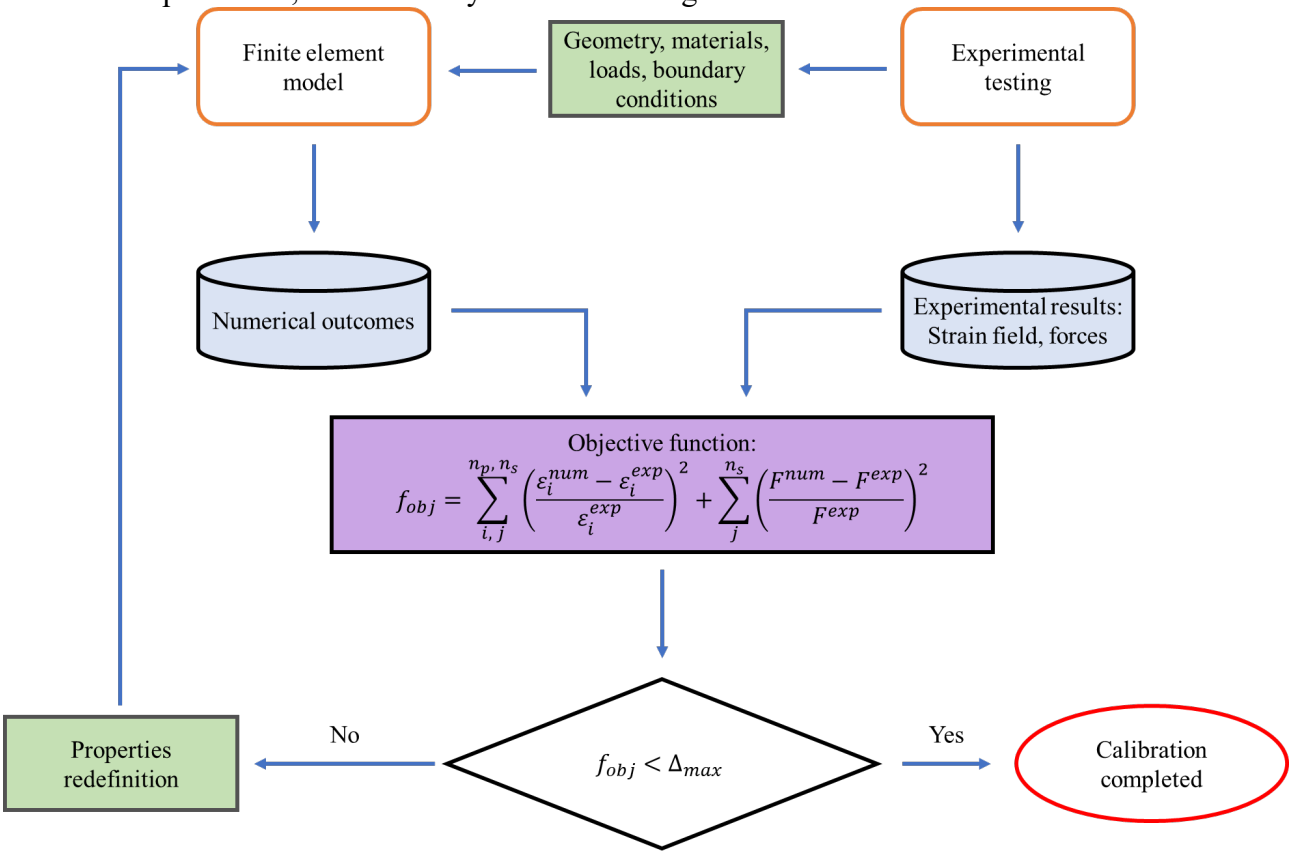


*Figure 2. Iterative procedure for parameters identification by finite elements model updating procedure.*

The procedure starts with a first attempt for material properties. The tensile testing is simulated by a finite element model using the ABAQUS numerical suite. The static mechanical analysis is performed on the reproduction of half sample for computational convenience, applying symmetry

boundary conditions at the sample middle edge, which corresponds to the welding centerline. The sample is partitioned in four zones characterized by different mechanical properties, namely the nugget zone, the thermo-mechanically affected zone, the heat affected zone, and the unaltered base material. In agreement with previous studies [29], the plastic behavior of the nugget zone and of the unaltered base material are not dependent on the position, and therefore are uniform in their zones. Vice versa, the properties in the thermo-mechanically affected zone and in the heat affected zone are linearly variable with the distance from the welding centerline. Of course, the plastic behavior cannot exhibit spatial discontinuity, therefore at the both the sides of each boundary between two zones the plastic properties are equal. The plastic behavior of each point is mathematically described by the Swift's law, described as

$$\sigma(\bar{\varepsilon}^{\mathrm{p}}) = k(\varepsilon_0 + \bar{\varepsilon}^{\mathrm{p}})^n \text{ , with } \varepsilon_0 = \left(\frac{\sigma_0}{k}\right)^{\frac{1}{n}} . \quad (1)$$

The sample discretized by shell elements and the applied boundary conditions are represented in Figure 3.

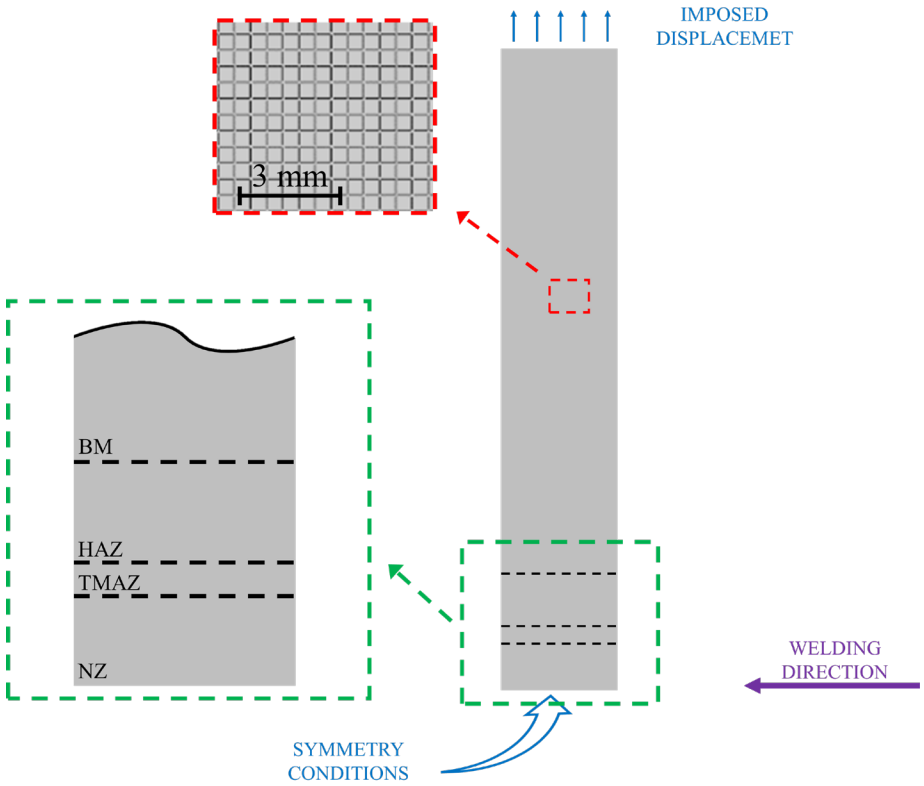


*Figure 3. Representation of the numerical domain, boundary conditions, and discretization of the finite element model.*

In each iteration, the numerical model computes the strain field and the applied tensile force considering the material's properties adopted. The objective function compares the numerical and experimental outcomes as

$$f_{obj} = \sum_{i,\ j}^{n_p,\ n_s} \left(\frac{\varepsilon_i^{num} - \varepsilon_i^{exp}}{\varepsilon_i^{exp}}\right)^2 + \sum_j^{n_s} \left(\frac{F^{num} - F^{exp}}{F^{exp}}\right)^2, \quad (2)$$

where $n_p$ is the number of available points and $n_s$ is the number of time steps.

Until the error of the numerical results overcome the maximum tolerance $\Delta_{max}$, the plastic parameters are iteratively redefined aiming to minimize the value of $f_{obj}$. The plastic behavior correction consists in a redefinition of the parameters k, $\sigma_0$, and n of Eq. 1.

The samples for microhardness testing have been embedded in mounting resin exposing the welding cross-section surface. The microindentations have been performed using a Leica VMHT-auto microhardness tester, using an indentation load of 100 g. The microhardness measurements have been carried out along with a 30 mm long path having its middle point at the welding centerline.

## Results and Discussion

The strain field evaluated in the tensile testing of the friction stir welded blanks samples is variable, depending on the distance from the welding centerline, as depicted in Figure 4.

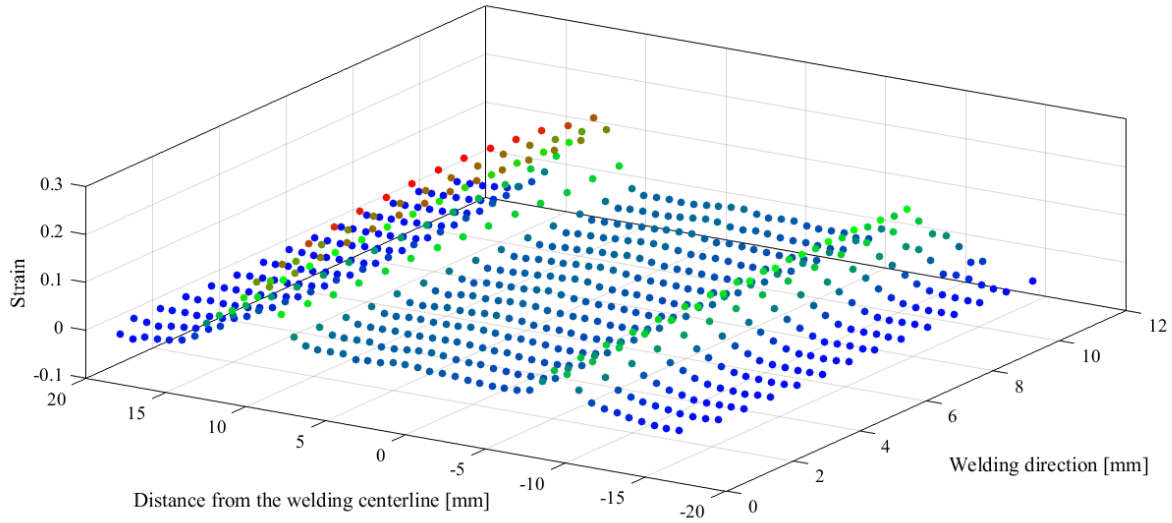


*Figure 4. Strain distribution in the welding line zone evaluated by DIC for the sample produced at 1000 rpm / 40 mm/min.*

As visible in Figure 4, two peaks of strain are visible on the sides of the welding line, in correspondence with the limit between thermo-mechanically affected zone and heat affected zone, as observed in previous works. The strain field evaluated at the nugget zone present higher values when compared to the deformations of the unaltered base material.

The FEMU is based on the iterative correction of the materials' elastoplastic parameters until the difference between the numerically computed values and the experimental measurement is lower than an acceptable tolerance. In Figure 5 numerical and experimental strain are compared.

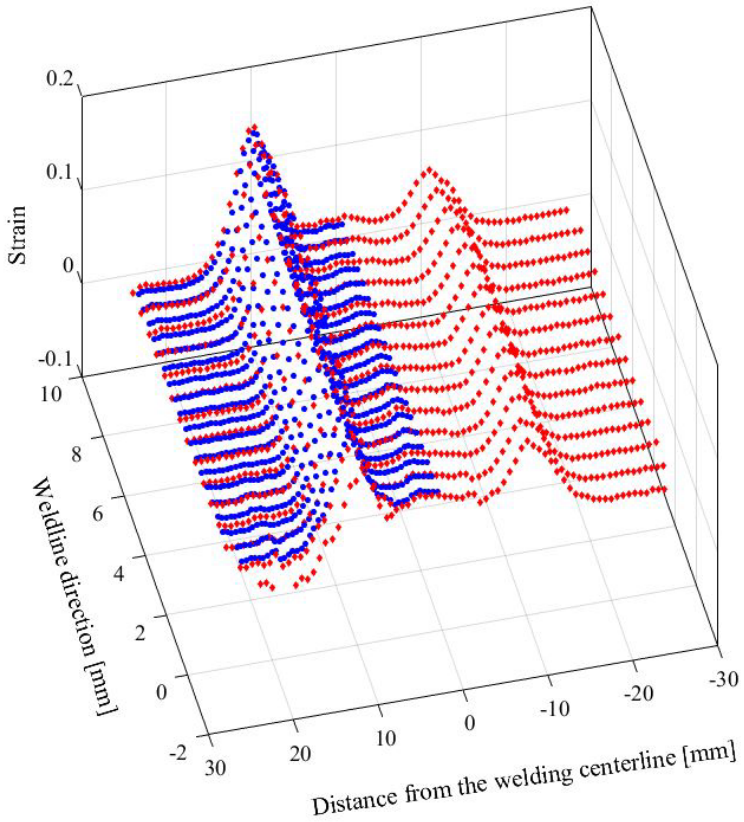


*Figure 5. Strain field: Comparison between experimental measurements (red points) and numerical results (blue points) for the sample produced at 1200 rpm / 70 mm/min.*

It is visible an asymmetry in the strain peaks depicted in the experimental results due to the different mechanisms characterizing the retreating and the advancing side in FSW. The calibration presented in this work regards just the side presenting the higher strain peak. Future works will consider the entire tailored blank. The FEMU has been used to evaluate the parameters of the Swift's law in the five different cases. In agreement with the strain behavior observed and reported in Figure 4 and 5, the plastic parameters have been considered constant in the nugget zone and in the unaltered base material, while they have been modeled linearly variable with the distance from the welding centerline in the thermo-mechanically affected zone and in the heat affected zone. Such parameters, namely $k$, $\sigma_0$, and $n$, evolves according to the evolution depicted in Figure 6.

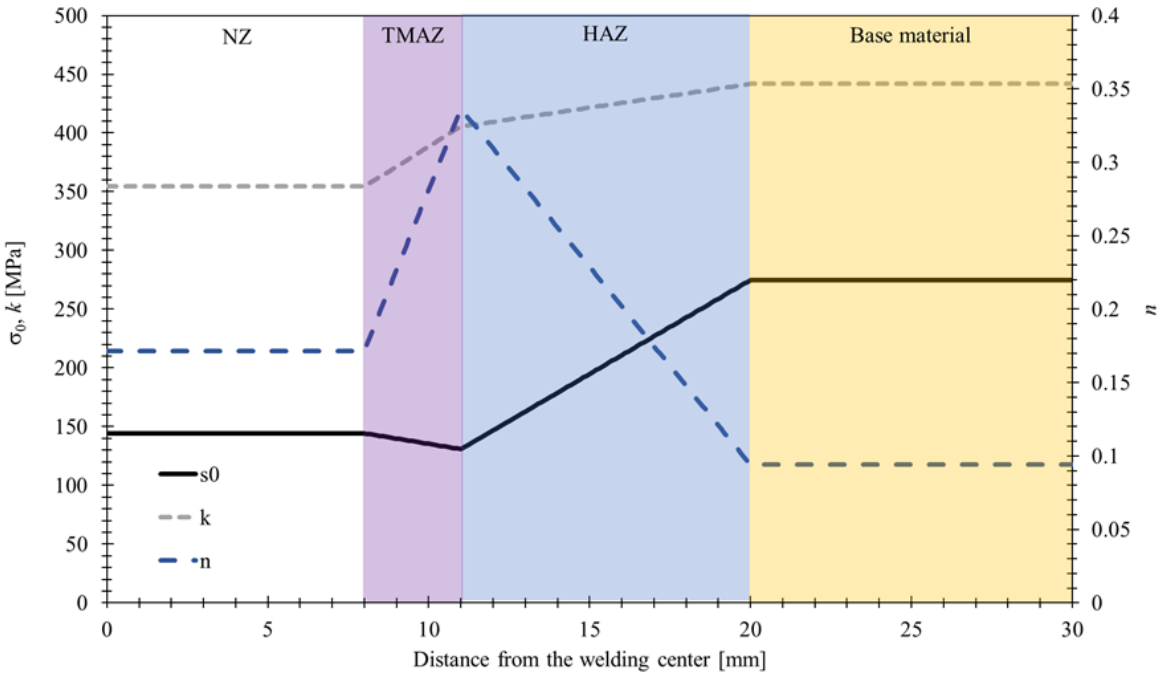


*Figure 6. Variation of the Swift's law parameters with the distance from the welding centerline for the representative case of tool rotational speed of 1000 rpm and advancing velocity of 100 mm/min.*

In order to completely describe the profiles depicted in Figure 6, just three values per each of the parameters should be reported, namely the nugget zone value, the unaltered base material value and the value at the boundary between thermo-mechanically affected zone and heat affected zone. The values in the different cases are reported in Table 2.

*Table 2. Swift's law parameters calibrated values.*

| | | $k\ [MPa]$ | $\sigma_0\ [MPa]$ | $n$ |
|---|---|---|---|---|
| 1000 rpm 40 mm/min | NZ | 346.6 | 147.8 | 0.261 |
| | TMAZ-HAZ | 422.0 | 82.4 | 0.407 |
| | BM | 441.7 | 274.8 | 0.094 |
| 1000 rpm 100 mm/min | NZ | 354.4 | 144.4 | 0.172 |
| | TMAZ-HAZ | 405.5 | 130.8 | 0.337 |
| | BM | 441.7 | 274.8 | 0.094 |
| 1200 rpm 70 mm/min | NZ | 346.5 | 157.1 | 0.242 |
| | TMAZ-HAZ | 420.3 | 105.7 | 0.352 |
| | BM | 441.7 | 274.8 | 0.094 |

The analysis of the microhardness confirms the behavior evidenced by the tensile testing and the strain analysis. Figure 7 reports the microhardness profiles in the five experimented cases.

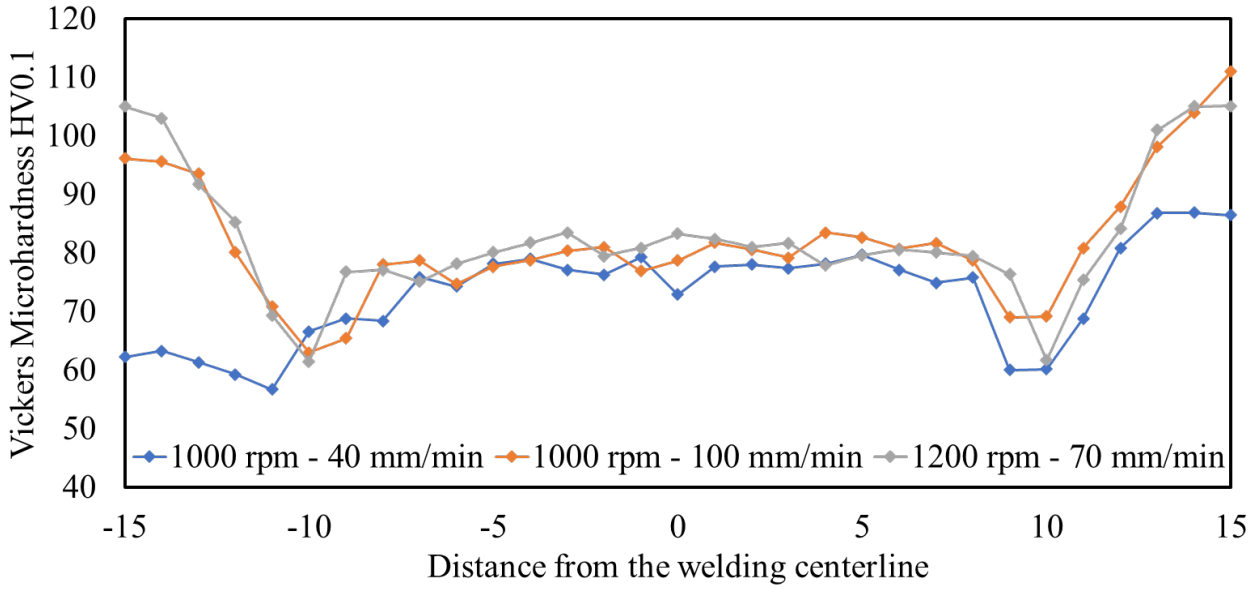


*Figure 7. Microhardness measurements on the friction stir welding cross-section surface.*

The value of microhardness along with the nugget zone (within a distance of 8 mm from the welding centerline) keeps constant value, while linearly decreasing and successively linearly increasing behaviors are observable respectively in the thermo-mechanically affected zone (from 8 mm to 11 mm from the welding centerline) and in the heat affected zone.

## Conclusions

This work presents the plastic properties calibration for friction stir welded tailored blanks in aluminum alloy AA6082 T6. The tensile testing with digital image correlation evidenced the differences in material properties due to the different FSW parameters, evidencing the effects related to the advancing velocity and the rotational speed of the tool. The differences are related to the combination of the mechanical stirring effects and the heating-cooling cycle dictated by the process. The constitutive law, modeled adopting the Swift's law, has been calibrated in the different cases by FEMU. The microhardness profiles of the friction stir welded blanks around the stirring zone confirm the elasto-plastic behavior observed in the tensile testing.

## Acknowledgments

The activities conducted have been promoted by the "ESAFORM mobility grant", which funded the mobility of the author Fausto Tucci to the University of Aveiro under the scientific supervision of Prof. Andrade Campos from the receiving institution and Prof. Carlone from the sending institution (University of Salerno).

## References

[1] Della Gatta R, Viscusi A, Perna AS, Caraviello A, Astarita A. Cold spray process for the production of AlSi10Mg coatings on glass fibers reinforced polymers. Mater Manuf Process 2021;36:106–21. doi:10.1080/10426914.2020.1813895.

[2] Viscusi A. Numerical investigations on the rebound phenomena and the bonding mechanisms in cold spray processes. AIP Conf Proc 2018;1960. doi:10.1063/1.5034957.

[3] Viscusi A, Astarita A, Carrino L, D'Avino G, de Nicola C, Maffettone PL, et al. Experimental study and numerical investigation of the phenomena occurring during long duration cold spray deposition. Int Rev Model Simulations 2018;11:84–92. doi:10.15866/iremos.v11i2.13619.

[4] Formisano A, Barone A, Carrino L, De Fazio D, Langella A, Viscusi A, et al. Improvement of the mechanical properties of reinforced aluminum foam samples. AIP Conf Proc 2018;1960. doi:10.1063/1.5034947.

[5] Silvestri AT, Papa I, Rubino F, Squillace A. On the critical technological issues of CFF: enhancing the bearing strength. Mater Manuf Process 2021;00:1–13. doi:10.1080/10426914.2021.1954195.

[6] Hassanin A El, Troiano M, Scherillo F, Silvestri AT, Contaldi V, Solimene R, et al. Rotation-assisted abrasive fluidised bed machining of alsi10mg parts made through selective laser melting technology. Procedia Manuf 2020;47:1043–9. doi:10.1016/j.promfg.2020.04.113.

[7] Hassanin A El, Troiano M, Silvestri AT, Contaldi V, Scherillo F, Solimene R, et al. Influence of abrasive materials in fluidised bed machining of AlSi10Mg parts made through selective laser melting technology. Key Eng Mater 2019;813 KEM:129–34. doi:10.4028/www.scientific.net/KEM.813.129.

[8] Hassanin A El, Velotti C, Scherillo F, Astarita A, Squillace A, Carrino L. Study of the solid state joining of additive manufactured components. RTSI 2017 - IEEE 3rd Int Forum Res Technol Soc Ind Conf Proc 2017. doi:10.1109/RTSI.2017.8065967.

[9] Rubino F, Ammendola P, Astarita A, Raganati F, Squillace A, Viscusi A, et al. An innovative method to produce metal foam using cold gas dynamic spray process assisted by fluidized bed mixing of precursors. Key Eng Mater 2015;651–653:913–8. doi:10.4028/www.scientific.net/KEM.651-653.913.

[10] Carlone P, Astarita A, Rubino F, Pasquino N, Aprea P. Selective Laser Treatment on Cold-Sprayed Titanium Coatings: Numerical Modeling and Experimental Analysis. Metall Mater Trans B Process Metall Mater Process Sci 2016;47:3310–7. doi:10.1007/s11663-016-0636-7.

[11] Vedernikov A, Safonov A, Tucci F, Carlone P, Akhatov I. Pultruded materials and structures: A review. J Compos Mater 2020;54:4081–117. doi:10.1177/0021998320922894.

[12] Rubino F, Nisticò A, Tucci F, Carlone P. Marine application of fiber reinforced composites: A review. J Mar Sci Eng 2020;8. doi:10.3390/JMSE8010026.

[13] Rubino F, Esperto V, Tucci F, Carlone P. Flow enhancement in liquid composite molding processes by online microwave resin preheating. Polym Eng Sci 2020;60:2377–89. doi:10.1002/pen.25477.

[14] Tucci F, Bezerra R, Rubino F, Carlone P. Multiphase flow simulation in injection pultrusion with variable properties. Mater Manuf Process 2020;35:152–62. doi:10.1080/10426914.2020.1711928.

[15] Rubino F, Pisaturo M, Senatore A, Carlone P, Sudarshan TS. Tribological Characterization of SiC and B4C Manufactured by Plasma Pressure Compaction. J Mater Eng Perform 2017;26:5648–59. doi:10.1007/s11665-017-3016-9.

[16] Rubino F, Tucci F, Esperto V, Perna AS, Astarita A, Carlone P, et al. Metallization of fiber reinforced composite by surface functionalization and cold spray deposition. Procedia Manuf 2020;47:1084–8. doi:10.1016/j.promfg.2020.04.353.

[17] Parmar H, Tucci F, Carlone P, Sudarshan TS. Metallisation of polymers and polymer matrix composites by cold spray : state of the art and research perspectives. Int Mater Rev 2021;0:1–25. doi:10.1080/09506608.2021.1954805.

[18] Parmar H, Khan T, Tucci F, Umer R, Carlone P. Advanced robotics and additive manufacturing of composites: towards a new era in Industry 4.0. Mater Manuf Process 2021. doi:10.1080/10426914.2020.1866195.

[19] Vedernikov A, Safonov A, Tucci F, Carlone P, Akhatov I. Modeling Spring-In of L-Shaped Structural Profiles Pultruded at Different Pulling Speeds. Polymers (Basel) 2021;13. doi:10.3390/polym13162748.

[20] Rubino F, Carlone P. A semi-analytical model to predict infusion time and reinforcement thickness in VARTM and SCRIMP processes. Polymers (Basel) 2019;11. doi:10.3390/polym11010020.

[21] Merklein M, Johannes M, Lechner M, Kuppert A. A review on tailored blanks - Production, applications and evaluation. J Mater Process Technol 2014;214:151–64. doi:10.1016/j.jmatprotec.2013.08.015.

[22] Tucci F, Carlone P, Silvestri AT, Parmar H, Astarita A. Dissimilar friction stir lap welding of AA2198-AA6082: Process analysis and joint characterization. CIRP J Manuf Sci Technol 2021;35:753–64. doi:10.1016/j.cirpj.2021.09.007.

[23] Astarita A, Tucci F, Silvestri AT, Perrella M, Boccarusso L, Carlone P. Dissimilar friction stir lap welding of AA2198 and AA7075 sheets: forces, microstructure and mechanical properties. Int J Adv Manuf Technol 2021;117:1045–59. doi:10.1007/s00170-021-07816-7.

[24] Mehta K, Astarita A, Carlone P, Della Gatta R, Vyas H, Vilaça P, et al. Investigation of exit-hole repairing on dissimilar aluminum-copper friction stir welded joints. J Mater Res Technol 2021;13:2180–93. doi:10.1016/j.jmrt.2021.06.019.

[25] Duflou JR, Habraken AM, Cao J, Malhotra R, Bambach M, Adams D, et al. Single point incremental forming: state-of-the-art and prospects. Int J Mater Form 2018;11:743–73. doi:10.1007/s12289-017-1387-y.

[26] Rubino F, Esperto V, Paulo RMF, Tucci F, Carlone P. Integrated manufacturing of AA6082 by friction stir welding and incremental forming: Strain analysis of deformed samples. Procedia Manuf 2020;47:440–4. doi:10.1016/j.promfg.2020.04.331.

[27] Carlone P, Thuillier S, Andrade-Campos A, de Sousa RJA, Valente R. Incremental forming of friction-stir welded aluminium blanks: an integrated approach. Int J Mater Form 2021;14:1121–37. doi:10.1007/s12289-021-01628-6.

[28] Tucci F, Andrade-Campos A, Thuillier S, Carlone P. On the Elastoplastic Behavior of Friction Stir Welded Tailored Blanks for Single Point Incremental Forming. ESAFORM 2021 2021:173376. doi:10.25518/esaform21.437.

[29] Andrade-Campos A, Thuillier S, Martins J, Carlone P, Tucci F, Valente R, et al. Integrated design in welding and incremental forming: Material model calibration for friction stir welded blanks. Procedia Manuf 2020;47:429–34. doi:10.1016/j.promfg.2020.04.327.

[30] Lan H, Venkatesh TA. On the relationships between hardness and the elastic and plastic properties of isotropic power-law hardening materials. Philos Mag 2014;94:35–55. doi:10.1080/14786435.2013.839889.

[31] Wang L, Ganor M, Rokhlin SI. Inverse scaling functions in nanoindentation with sharp indenters: Determination of material properties. J Mater Res 2005;20:987–1001. doi:10.1557/JMR.2005.0124.